# FEATURE ARTICLE

## Spectroscopy and Dynamics of Fast Evolving States

C. X. W. Qian,† A. Ogai, J. Brandon, Y. Y. Bai, and H. Reisler*

*Department of Chemistry, University of Southern California, Los Angeles, California 90089-0482*
*(Received: April 22, 1991)*

This article describes several aspects of the spectroscopy and dynamics of photodissociating molecules. In particular, we report both experimental studies and theoretical models relating to the mapping of transition-state wave functions into fragment rotational distributions. A modified Franck–Condon model is described in detail for cases of modest exit-channel torques, and is applied to the dissociation of $ClNO(T_1)$, where several bending progressions are identified in the $T_1$ dissociative state. The mapping of the wave functions in the case of large exit-channel torques are demonstrated in the dissociation of $ClNO(S_1)$ and $FNO(S_1)$. Favorable cases for mapping of parent ground- and excited-state bending wave functions into product distributions are then identified. We also describe the spectroscopic assignments of dissociative states of ClNO. Photofragment yield spectra, NO energy distributions and vector properties are used, as well as results of ab initio calculations of singlet and triplet excited states and oscillator strengths. It is concluded that definitive assignments are now possible for dissociative spectra of many small polyatomic molecules. The adiabatic evolution of NO stretch excitation into NO vibration in the dissociation of ClNO on $T_1$ and $S_1$ is also briefly described. The interplay between theory and experiment is emphasized throughout.

### 1. Introduction

Photodissociation dynamics is a mature and popular field that still attracts considerable attention owing to the obvious simplifications inherent in "half-collision" processes, and the relative ease with which products are detected state-selectively.[1] These simplifications have led to a large body of work on many molecules and no single review today can cover the field in its entirety. The initial enthusiasm generated by the simplicity of half-collision processes (as compared with the "full collisions" of reactive encounters) soon gave way to a realization that the ensuing dynamics is so intimately dependent on the details of a particular potential energy surface (PES) that each molecule becomes a "subspecialty". If the photodissociation dynamics depends strongly on the details of each molecular PES, there is little hope of finding trends that can be described by general theories.

Fortunately, the abundant experimental and theoretical output resulted in some general trends that govern exit-channel interactions. In particular, work on molecules such as $H_2O$,[1c,2,3] HONO,[4-6] RONO (R = alkyl),[1c,7] and XCN (X = Cl, Br, I)[1e,8,9] led to formulations of models that describe product rotational and vibrational excitations, while work on $CH_3X$ (X = I, Br)[1e,10,11] XCN,[1e,12] and $HN_3$[13,14] has highlighted the importance of surface crossings and conical intersections and their influence on product state distributions. Today, owing both to experimental and theoretical developments, it is possible to design experiments that probe fundamental issues using prototypical molecules, and compare them with quantum mechanical and classical dynamical calculations on multidimensional potential energy surfaces (PES) calculated ab initio. Triatomic molecules have traditionally served as benchmarks for testing ideas and theories, since the internal excitations of the diatomic fragment can be interrogated with great precision, and good ab initio calculations of the PES's are feasible in many cases.

The purpose of the present article is to highlight two aspects of photodissociation dynamics as recently demonstrated in our work. First, we will show how, with a combination of measured scalar and vector properties of the fragments and ab initio calculations of the parent PES's, it is possible to assign definitively dissociative spectra that lack traditional rotational and vibrational structure. Moreover, with optimized ab initio calculations, avoided crossings and conical intersections along the reaction coordinate can be identified, as well as changes in the excited-state geometry

† Present address: Laser Chemistry Group, Steacie Institute for Molecular Sciences, National Research Council Canada, 100 Sussex Drive, Ottawa, Ontario, K1A 0R6, Canada.

(1) For recent reviews see, for example: (a) Houston, P. L. *J. Phys. Chem.* **1987**, *91*, 5388. (b) Simons, J. P. *J. Phys. Chem.* **1987**, *91*, 5378. (c) Ashfold, M. N. R., Baggott, J. E., *R. Soc. Chem.* **1987**, 139. (d) Shapiro, M.; Bersohn, R. *Annu. Rev. Phys. Chem.* **1982**, *33*, 119. (e) Hall, G. E.; Houston, P. L. *Annu. Rev. Phys. Chem.* **1989**, *40*, 375. (f) Jackson, W. M.; Okabe, H. *Adv. Photochem.* **1985**, *13*, 1.

(2) (a) Andresen, P.; Schinke, R. In *Molecular Photodissociation Dynamics*; Baggott, J., Ashfold, M. N. R., Eds.; Royal Society of Chemistry: London, 1987. (b) Andresen, P.; Beushausen, V.; Häusler, D.; Lülf, H. W.; Rothe, E. W. *J. Chem. Phys.* **1985**, *83*, 1429. (c) Schinke, R.; Engel, V.; Andresen, P.; Häusler, D.; Balint-Kurti, G. G. *Phys. Rev. Lett.* **1985**, *55*, 1180.

(3) (a) Vander Wal, R. L.; Crim, F. F. *J. Phys. Chem.* **1989**, *93*, 5331. (b) Vander Wal, R. L.; Scott, J. L.; Crim, F. F. *J. Chem. Phys.* **1990**, *92*, 803. (c) Crim, F. F.; Hsiao, M. C.; Scott, J. L.; Sinha, A.; Vander Wal, R. L. *Philos. Trans. R. Soc.*, **1990**, *332*, 259.

(4) Vasudev, R.; Zare, R. N.; Dixon, R. N. *J. Chem. Phys.* **1984**, *80*, 4863.

(5) Dixon, R. N.; Rieley, H. *J. Chem. Phys.* **1989**, *91*, 2308, and references cited therein.

(6) Henning, S.; Untch, A.; Schinke, R.; Nonella, M.; Huber, J. R. *Chem. Phys.* **1989**, *129*, 93.

(7) (a) Nonella, M.; Huber, J. R. *Chem. Phys. Lett.* **1986**, *131*, 376. (b) Hennig, S.; Engel, V.; Schinke, R.; Nonella, M.; Huber, J. R. *J. Chem. Phys.* **1987**, *87*, 3522. (c) Nonella, M.; Huber, J. R.; Untch, A.; Schinke, R. *J. Chem. Phys.* **1989**, *91*, 194.

(8) Nadler, I.; Mahgarefteh, D.; Reisler, H.; Wittig, C. *J. Chem. Phys.* **1985**, *82*, 3885.

(9) Black, J. F.; Waldeck, J. R.; Zare, R. N. (a) *J. Chem. Phys.* **1990**, *92*, 3519; (b) *Mol. Phys.*, in press.

(10) Lao, K. Q.; Person, M. D.; Butler, L. J. *J. Chem. Phys.* **1988**, *89*, 3463.

(11) Person, M. D.; Lao, K. Q.; Eckholm, B. J.; Butler, L. J. *J. Chem. Phys.* **1989**, *91*, 812.

(12) (a) Goldfield, E. M.; Houston, P. L.; Ezra, G. S. *J. Chem. Phys.* **1986**, *84*, 3120. (b) Guo, H.; Schatz, G. C. *J. Chem. Phys.* **1990**, *92*, 1634. (c) Dugan, C. H.; Anthony, D. *J. Phys. Chem.* **1987**, *91*, 3929. (d) Heather, R.; Metiu, H. *Chem. Phys. Lett.* **1989**, *157*, 505. (e) Henriksen, N. E.; Heller, E. J. *J. Chem. Phys.* **1989**, *91*, 4700.

(13) (a) Foy, B. R.; Casassa, M. P.; Stephenson, J. C.; King, D. S. *J. Chem. Phys.* **1989**, *90*, 7037. (b) Foy, B. R.; Casassa, M. P.; Stephenson, J. C.; King, D. S. *J. Chem. Phys.* **1988**, *89*, 608.

(14) Alexander, M. H.; Werner, H. J.; Dagdigian, P. J. *J. Chem. Phys.* **1988**, *89*, 1388.

0022-3654/91/2095-6763$02.50/0 

during the dissociation. Two molecules may well represent two extreme cases: in ClNO, each repulsive PES evolves independently to products,[15] whereas in ClCN, several electronic configurations give rise to a dense manifold of electronic states and many opportunities for surface crossings along the Cl–C reaction coordinate exist.[16] Here, we will describe some of our studies on ClNO, while the ClCN results are reported elsewhere.[16]

A second aspect emphasized here is the generation of torque that leads to rotational excitation in photoproducts. In particular, we will describe in detail the mapping of parent transition-state bending wave functions into fragment rotational excitations recently observed in our laboratory. In general, the influence of parent internal excitations on product state distributions receives less experimental attention, since it is not easily probed. For example, when investigating the role of vibrational excitation in the *upper* electronic state, we rely on a serendipitous matching of timings—the molecule in the electronically excited state must live long enough to support a vibrational structure, while this time should be sufficiently short (i.e., "direct" photodissociation) to preserve the relationship between features of the excited PES and the subsequent dynamics. The nitrosyl halides exhibit a diffuse vibrational structure in their lowest electronic transitions, even though the upper states are repulsive and are therefore good candidates for these studies.

In direct dissociation of polyatomic molecules, parent *bending* vibrations usually evolve into fragment *rotational* excitations; however, this transformation is often mediated by the torques generated on the repulsive surface during dissociation. Thus, models need to be developed that provide physical insight into the relative importance of angular momentum sources. As usual, we do best in limiting cases, and early on two models describing different sources of torque that are *independent* of the details of the PES were developed. The Franck–Condon (FC) model of photodissociation was developed for those cases where parent vibrations are the *only* source of angular momentum.[17-20] In these cases the parent bending vibrations were expanded in terms of free-rotor wave functions of the fragments, subject to angular momentum couplings and conservation laws. The price of the exact treatments of angular momenta, however, was a set of complicated final equations from which the physics was not always apparent. At the other extreme is a situation where the most important source of torque is the impulsive force generated in the photoexcitation. For such a situation, a simple impulsive model was developed which assumed that the impulse is directed along the breaking bond, and no other sources of angular momenta are important.[21] As shown recently by Schinke, the impulsive model implies an evolution on a PES where the initial angular momentum is not modified along the reaction coordinate during dissociation.[21b]

Thus, the FC and impulsive models are limiting cases applicable when a single source of angular momentum is dominant (i.e., the bending vibration or the impulsive force, respectively), and the shape of the PES is unimportant. These models are useful, because they provide reference rotational distributions with which the experimental distributions can be compared, but they do not provide the more realistic models that experimentalists need. To this end, Schinke developed a model termed the rotational reflection principle,[22] which is highly successful when a large impulsive torque is dominant, whereas we used a modified FC model to deal with situations where exit-channel torques are nonnegligible, but nevertheless modest compared with the torques inherent in the parent bending wave functions.[23,24] Of course the best and most rigorous approach involves exact close-coupling quantum-mechanical calculations on realistic three-dimensional PES's calculated ab initio.[25-27] Such calculations, in principle, take into account all the forces and torques that influence fragment rotations. However, the physics is not always transparent, and in addition, accurate PES's are not readily available, and the calculations can be quite time consuming when many channels are open.

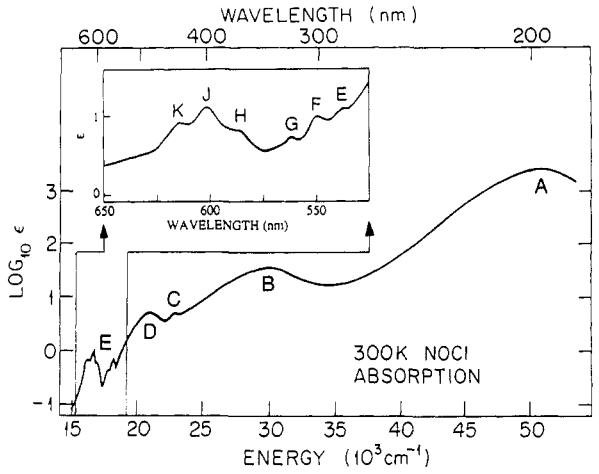


**Figure 1.** The absorption spectrum of 300 K ClNO as measured by Goodeve and Katz (ref 28). The lowest absorption band, denoted here the E band, corresponds to a series of diffuse bands (see inset) labeled E–K in ref 28.

**TABLE I: Molecular Orbitals Involved in the Lowest Excited States of ClNO[a]**

| symmetry | MO | eigenvalue, au | description |
|---|---|---|---|
| a′ | 18 | 0.0704 | Cl $p_x$ + NO $\pi_x^*$ |
| a″ | 17 | 0.0409 | NO $\pi_z^*$ |
| a′ | 16 | −0.4245 | Cl $p_x$ + O $p_x$ |
| a′ | 15 | −0.4516 | Cl $p_y$ |
| a″ | 14 | −0.4520 | Cl $p_z$ |
| a″ | 13 | −0.7323 | NO $\pi_z$ |

[a] From ref 15.

This article is organized as follows. We first discuss how we assigned the dissociative electronic spectrum of ClNO, and the implications of these assignments to the photodissociation dynamics. We then discuss in detail the mapping of bending wave functions into product rotational states when the bending wave function is the dominant source of torque, and describe the modified FC model and its application to the photodissociation of ClNO($T_1$). We use the dissociation of ClNO on $S_1$ as an example of direct dissociation involving large exit-channel torque which is nicely described by exact quantum mechanical and classical dynamical calculations. We conclude by demonstrating that transition-state wave functions can be mapped into product rotational distribution even in the presence of a *large* exit-channel torque [e.g., FNO($S_1$)], and commenting on the general applicability of the models.

## 2. Spectroscopy of Dissociating States of ClNO

The broad band, structureless electronic spectrum of ClNO, which was obtained in 1939 by Goodeve and Katz (Figure 1), illustrates the difficulty in assigning the transitions of dissociating states.[28] Goodeve and Katz named the peaks A–K in the order

(15) Bai, Y. Y.; Ogai, A.; Qian, C. X. W.; Iwata, L.; Segal, G. A.; Reisler, H. *J. Chem. Phys.* **1989**, *90*, 3903.
(16) Bai, Y. Y.; Segal, G. A.; Reisler, H. *J. Chem. Phys.* **1991**, *94*, 331.
(17) Morse, M. D.; Freed, K. F. (a) *J. Chem. Phys.* **1981**, *74*, 4395; (b) *Ibid.* **1983**, *78*, 6045; (c) *Chem. Phys. Lett.* **1980**, *74*, 49.
(18) Morse, M. D.; Freed, K. F.; Band, Y. B. (a) *J. Chem. Phys.* **1979**, *70*, 3604; (b) *Ibid.* **1979**, *70*, 3620.
(19) Beswick, J. A.; Gelbart, W. M. *J. Phys. Chem.* **1980**, *84*, 3148.
(20) Freed, K. F.; Band, Y. B. In *Excited States*; Lim, E., Ed.; Academic: New York, 1978; Vol. 3.
(21) (a) Tuck, A. F. *J. Chem. Soc. Faraday Trans. 2* **1977**, *73*, 689. (b) Schinke, R. *Comments At. Mol. Phys.* **1989**, *23*, 15. (c) Busch, G. E.; Wilson, K. R. *J. Chem. Phys.* **1972**, *56*, 3626.
(22) (a) Schinke, R. *J. Phys. Chem.* **1986**, *90*, 1742. (b) Schinke, R.; Engel, V. *Faraday Discuss. Chem. Soc.* **1986**, *No. 82*, 111.
(23) Qian, C. X. W.; Ogai, A.; Iwata, L.; Reisler, H. *J. Chem. Phys.* **1990**, *92*, 4296.
(24) Qian, C. X. W.; Reisler, H. In *Advances in Molecular Vibrations and Collision Dynamics*; Bowman, Joel M., Ed.; JAI Press, Inc.: London, in press.
(25) Balint-Kurti, G. G.; Shapiro, M. *Photodissociation Photolon.* **1985**, 403.
(26) Schinke, R. *Annu. Rev. Phys. Chem.* **1988**, *39*, 39.
(27) Balint-Kurti, G. G.; Shapiro, M. *Chem. Phys.* **1981**, *61*, 137.

**TABLE II: Vertical Excitation Energies and Oscillator Strengths for ClNO[a]**

| state | primary excitation | $E_{calc}$, eV | $E_{exp}$,[b] eV | $f_{calc}$ | $f_{exp}$[c] | band |
|---|---|---|---|---|---|---|
| $S_0(1^1A')$ | | 0.0 | | 0.0 | | |
| $T_1(1^3A'')$ | $17a'' \leftarrow 16a'$ | 1.75 | 2.06 | 0.0 | $1 \times 10^{-5}$ | E |
| $S_1(1^1A'')$ | $17a'' \leftarrow 16a'$ | 2.32 | 2.64 | $2 \times 10^{-4}$ | $9 \times 10^{-5}$ | D, C |
| $T_2(1^3A')$ | $18a' \leftarrow 16a'$ | 2.90 | | 0.0 | | |
| $T_3(2^3A')$ | $17a'' \leftarrow 14a''$ | 3.13 | | 0.0 | | |
| $T_4(2^3A'')$ | $17a'' \leftarrow 15a'$ | 3.29 | | 0.0 | | |
| $S_2(2^1A'')$ | $17a'' \leftarrow 15a'$ | 3.37 | | $8 \times 10^{-6}$ | | |
| $S_3(2^1A')$ | $17a'' \leftarrow 14a''$ | 3.70 | 3.72 | $1 \times 10^{-1}$ | $1 \times 10^{-3}$ | B |
| $T_5(3^3A')$ | $18a' \leftarrow 15a'$ | 4.48 | | 0.0 | | |
| $S_4(3^1A')$ | $18a' \leftarrow 15a'$ | 4.79 | | $1 \times 10^{-3}$ | | |
| $S_5(4^1A')$ | $18a' \leftarrow 16a'$ | 7.18 | 6.30 | 1.0 | 0.5 | A |

[a] From ref 15; energies relative to $1^1A'$ $E_{eq} = -589.153\,392$ au at the experimental equilibrium geometry; $r_{NCl} = 1.975$ Å, $r_{NO} = 1.13$ Å, ∠ClNO = 113.3°. [b] $E_{exp}$ is defined as the peak of the absorption band. [c] The experimental oscillator strengths were calculated from the spectra and extinction coefficients given in ref 28.

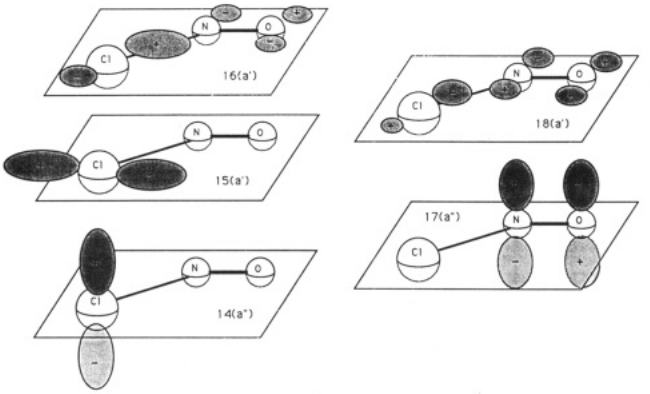


**Figure 2.** A pictorial view of the relevant occupied and unoccupied orbitals involved in the electronic transitions of ClNO. A fuller description of each orbital is given in Table I.

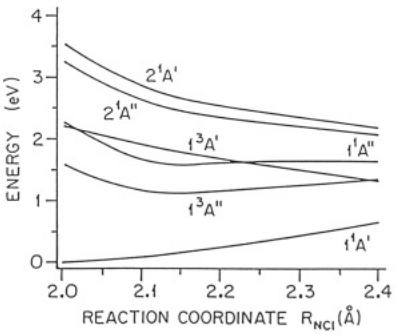


**Figure 3.** Optimized least energy paths for ClNO along the reaction coordinate, $r_{ClN}$, obtained by optimizing $r_{NO}$ and the ClNO angle.

of increasing wavelength and were able, by inspection, to make suggestions on possible assignments, some of which eventually proved to be correct. For example, they proposed that the lowest, weak absorption peaks labeled E–K (see inset in Figure 1) belong to a single electronic transition and that this transition, due to its weakness, may be forbidden. In order to assign the electronic spectrum we used vector and scalar properties of the fragments and also carried out ab initio calculations on the low-lying states of ClNO.[15] Our calculations were more complete than previous ones[29] in that we included triplet states, calculated oscillator strengths, and carried out more complete explorations of the PES's along the reaction coordinate.

The experimental ground-state equilibrium geometry of the bent ClNO is $r_{NO} = 1.13$ Å, $r_{ClN} = 1.975$ Å, and ∠ClNO = 113.3°.[30] ClNO has 18 valence electrons, and 16 molecular orbitals are occupied in the ground state. In our coordinate system, the $y$ axis is along the NO bond, and Cl lies in the $xy$ plane. At infinite separation, NO possesses doubly degenerate $\pi$ and $\pi^*$ molecular orbitals that may be viewed as lying in the $x$ and $z$ directions. The molecular orbitals (MO's) which are principally involved in the excited states are summarized in Table I, and a pictorial view is given in Figure 2.[15] The highest occupied MO's, 14–16, are predominantly the three Cl p orbitals which are degenerate in the atom and nearly degenerate in ClNO. Excitations from these to MO 17, which is predominantly of NO $\pi_z^*$ character, lie close to each other in energy and this accounts for the richness of the spectrum below 4 eV.

The calculated vertical excitation energies and the electric dipole oscillator strengths are summarized in Table II.[15] The lowest excited states all involve some degree of charge transfer from Cl to NO.[15] The dynamics of the photofragmentation of ClNO to $Cl(^2P_{1/2,3/2})$ and $NO(^2\Pi_{1/2,3/2})$ depends upon the nature of the three-dimensional PES upon which dissociation takes place. Therefore, the calculated least energy paths for a number of electronic states, where $r_{NO}$ and the ClNO angle are optimized as a function of $r_{ClN}$, are shown in Figure 3.[15]

As seen in Table II, we assign the lowest energy absorption system to the $T_1 \leftarrow S_0$ transition, and both the D and C bands to the $S_1 \leftarrow S_0$ transition. We emphasize that without the interplay between theory and experiment, it would have been impossible to propose definitive assignments for the dissociative transitions. Below, we discuss some of the considerations that led to the spectroscopic assignments of the lowest triplet and singlet states. The assignments of the other transitions are described elsewhere.[15,24]

On the basis of its vertical excitation energy and oscillator strength, we assigned the D absorption band to the $S_1(1^1A'') \leftarrow S_0(1^1A')$ transition. The Doppler profiles of selected NO rovibrational levels following excitation in the D band are shown in the middle panel of Figure 4, and indicate that $\mu$ is perpendicular to v ($\beta \cong -1$).[15,31,32] The rotational alignment parameter indicates that the transition is of a perpendicular nature, with $\mu$ perpendicular to the molecular plane, thereby establishing the symmetry of the upper electronic state as A".[15,33,34] The $NO(^2\Pi_{1/2})$ Λ-doublet populations, which yield $\Pi(A'') > \Pi(A')$,[32,35,36] are consistent with this assignment, since excitation is predominantly to MO 17 whose symmetry is a", as is the overall symmetry of the transition.

More intriguing is the assignment of the C band to the same electronic transition as the D band. This assignment was proposed by us based solely on experimental observations of scalar and vector properties of the NO fragment.[15] For example, NO pro-

(28) Goodeve, C. F.; Katz, S. *Proc. R. Soc.* (*London*) **1939**, *A172*, 432.
(29) Solgadi, D.; Lahmani, F.; Lardeux, C.; Flament, J. P. *Chem. Phys.* **1983**, *79*, 225.
(30) Millen, D. J.; Pannell, J. *J. Chem. Soc.* **1961**, 1322.
(31) (a) Zare, R. N.; Herschbach, D. R. *Proc. IEEE* **1963**, *51*, 173. (b) Zare, R. N. *Mol. Photochem.* **1972**, *4*, 1.
(32) Bruno, A. E.; Bruhlmann, U.; Huber, J. R. *Chem. Phys.* **1988**, *122*, 155.
(33) Greene, C. H.; Zare, R. N. *Annu. Rev. Phys. Chem.* **1982**, *33*, 119.
(34) Greene, C. H.; Zare, R. N. *J. Chem. Phys.* **1983**, *78*, 6741.
(35) (a) Andresen, P.; Rothe, E. W. *J. Chem. Phys.* **1985**, *82*, 3634. (b) Alexander, M. H.; Dagdigian, P. J. *J. Chem. Phys.* **1984**, *80*, 4863. (c) Alexander, M. H., et al. *J. Chem. Phys.* **1988**, *89*, 1749.
(36) Ogai, A.; Qian, C. X. W.; Iwata, L.; Reisler, H. *Chem. Phys. Lett.* **1988**, *146*, 367.

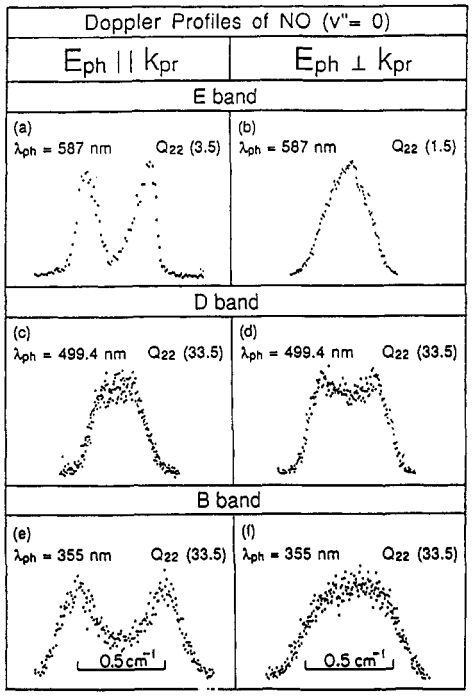


**Figure 4.** Doppler profiles of NO($X^2\Pi_{3/2}$, $v''=0$) $Q_{22}$ lines from dissociation of ClNO. The left- and right-hand side entries are associated with $E_{ph}$ parallel and perpendicular, respectively, to $k_{pr}$. The lasers configuration in all the panels except (b) is $k_{pr} \perp k_{ph}$. In panel (b) $k_{pr} \parallel k_{ph}$ was employed. This affects the Doppler profiles only through the $v$–$J$ correlation, and has only a small effect on the line shape.

duced via photolysis in both the D and C bands exhibits similar Doppler profiles, degree of rotational alignment, Λ-doublet propensities, and rotational distributions, provided NO($v''=0$) is monitored with D band excitation, and NO($v''=1$) is monitored following excitation in the C band. Moreover, the two peaks are separated by 1500 $cm^{-1}$, which is typical of molecular NO stretch vibration. Recently, this assignment has been confirmed by exact dynamical calculations on a three-dimensional $S_1$ PES calculated ab initio.[37] The calculations show two peaks identical with the D and C absorption bands observed with jet-cooled samples (Figure 5).[38] The calculations also predict that excitations in the D and C bands yield NO in $v'' = 0$ and 1, respectively, as observed experimentally.[15,38] Thus, the bands labeled D and C in the original spectrum (i.e., those peaking at ~472 and 440 nm)[28] arise from the $S_1(1^1A'') \leftarrow S_0(1^1A')$ transition terminating in the (000) and (100) $S_1$ levels, respectively.

We now turn our attention to the series of weak bands designated E–K in ref 28 (i.e., the E band), which we assign as the $T_1(1^3A'') \leftarrow S_0(1^1A')$ transition. With excitation in the E band, the recoil anisotropy parameter is typical of a parallel transition, as can be seen clearly by comparing the Doppler profiles displayed in the upper panel of Figure 4 with those of the B band (lowest panel), which is known to involve a parallel transition. The rotational alignment parameter also implies that $\mu$ must lie in the molecular plane. The oscillator strength, however, is quite small, and Goodeve and Katz already suggested that it may involve a forbidden transition.[28] We ascribe this transition to spin–orbit coupling between the $T_1(1^3A'')$ state and higher lying and strongly absorbing singlet states of A′ symmetry.[15] By calculating the first-order mixing coefficients between the $1^3A''$ state and singlet states of A′ symmetry,[39] we find that the observed oscillator strength of the $T_1 \leftarrow S_0$ transition (~$10^{-5}$) can be accounted for by intensity borrowing from the strong ($f \sim 0.5$), parallel $S_5(4^1A') \leftarrow S_0(1^1A')$ transition (i.e., the A band).[15] We emphasize that

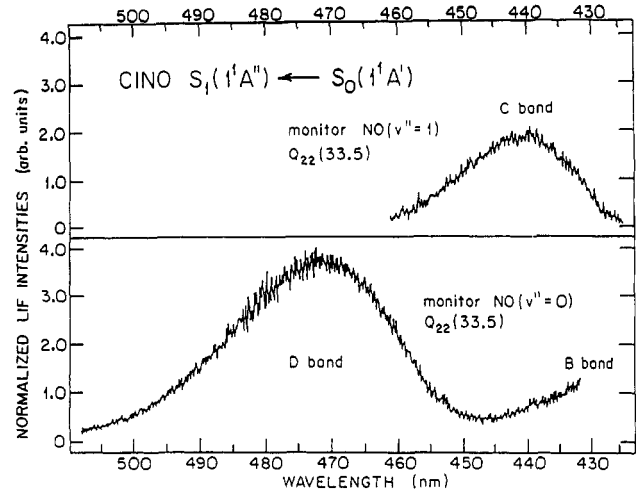


**Figure 5.** Photofragment yield (PHOFRY) spectra in the region of $S_1 \leftarrow S_0$ ClNO excitation. The upper panel obtained by monitoring NO($v''=1$) shows a peak corresponding to the C band in the absorption spectrum. This peak does not appear in the lower panel when NO($v''=0$) is monitored. The intensities of the bands are normalized to each other and reflect the relative partial absorption cross sections. In both spectra, the $Q_{22}(33.5)$ line was monitored.

although mixings with singlet states are responsible for the oscillator strength and thus determine the values of $\beta$ and $A_0^{(2)}$, only ~2% of the $4^1A'$ wave function is required to yield the experimentally observed oscillator strength. Thus, the $T_1$ state has predominantly $1^3A''$ character, and the Λ-doublet populations indeed reflect the a″ symmetry of the excited-state orbital (MO 17).[15]

In summary, the following assignments are now favored for the electronic spectrum of ClNO in the 625–180-nm-wavelength region.[15]

1. $T_1(1^3A'') \leftarrow S_0(1^1A')$ (E band); $\nu_1' = 1500\ cm^{-1}$, $\nu_3' = 380\ cm^{-1}$. A series of weak bands with diffuse structure at ~625–500 nm. The transition borrows intensity by mixing with remote singlet states, predominantly the $S_5(4^1A')$ state.
2. $S_1(1^1A'') \leftarrow S_0(1^1A')$ (D and C bands); two peaks at 472 and 440 nm, corresponding to $\nu_1' = 1500\ cm^{-1}$.
3. $S_3(2^1A') \leftarrow S_0(1^1A')$ (B band); a strong, broad band with no discernible structure, that peaks at ~340 nm.
4. $S_5(4^1A') \leftarrow S_0(1^1A')$ (A band); a very strong, broad band with no structure that peaks at ~200 nm. The upper state may be the $NO^+Cl^-$ charge-transfer state.

Better resolved spectra and additional information can be obtained from the state-specific photofragment yield (PHOFRY) spectra obtained by varying the photolysis laser wavelength while monitoring selected levels of NO($X^2\Pi$).[23] Several PHOFRY spectra in the $T_1 \leftarrow S_0$ band are shown in Figure 6 and compared with the 300 K absorption spectrum of ClNO. We find that when monitoring low rotational levels in NO($v''=0$), only the first group of three peaks is observed, whereas monitoring NO($v''=1$) yields only the second group of peaks (i.e., the ($00v_3$) and ($10v_3$) bending progressions, respectively). The reason, of course, is that the PHOFRY spectra exhibit only those transitions that correlate with the monitored states of the photofragments. Thus, the state-specific PHOFRY spectra can reveal absorption features that are hidden or overlapped in the total absorption spectrum. This is best illustrated by the PHOFRY spectrum obtained when NO($v''=2$) is monitored. The 300 K absorption spectrum at 450–525 nm shows the broad and structureless $S_1 \leftarrow S_0$ D band.[15,28] The PHOFRY spectrum obtained when NO($v''=0$) is monitored reproduces the absorption spectrum very well. In contrast, when NO($v''=2$) is monitored, only weak features, consisting of the three peaks characteristic of the bending progressions of the $T_1 \leftarrow S_0$ transition, appear in the PHOFRY spectrum, as seen in Figure 6.[23] Thus the simultaneous absorption to $S_1$ and $T_1$ can be revealed only in the state-selective PHOFRY spectra. A similar situation exists in the spectral region around 430 nm, where the C and B bands overlap. The PHOFRY spectra, as well as the NO scalar

(37) (a) Schinke, R.; Nonella, M.; Suter, H.; Huber, J. R. *J. Chem. Phys.* **1990**, *93*, 1098. (b) Untch, A.; Weide, K.; Schinke, R. *J. Chem. Phys.*, submitted for publication.
(38) Ogai, A.; Qian, C. X. W.; Reisler, H. *J. Chem. Phys.* **1990**, *93*, 1107.
(39) Lefebvre-Brion, H.; Field, R. W. *Perturbations in the Spectra of Diatomic Molecules*; Academic: New York, 1986.

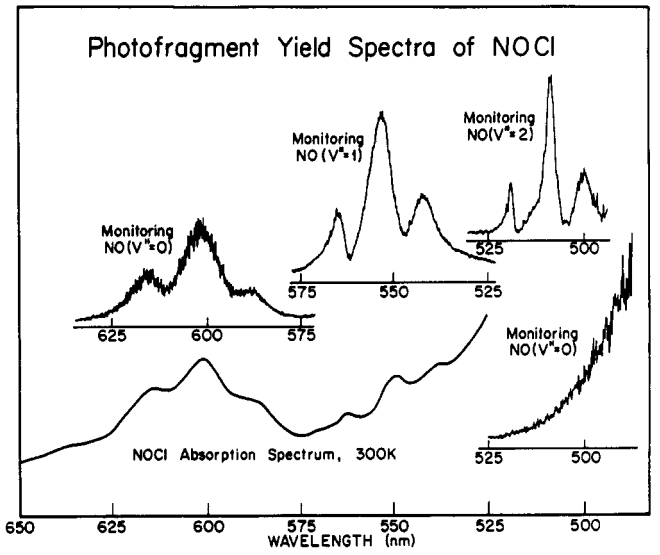


**Figure 6.** The absorption and PHOFRY spectra of ClNO in the region of the $T_1 \leftarrow S_0$ transition. The absorption spectrum was obtained at 300 K. The other traces show the PHOFRY spectra obtained with jet-cooled samples, and each group of three peaks was obtained by monitoring the $P_{22}$ bandhead ($J'' = 1.5$–$4.5$) of the NO vibrational level indicated in the figure. The first group consists of, in order of decreasing wavelength, the (000), (001), and (002) bands; the second group consists of the (100), (101), and (102) bands, and the third group consists of the (200), (201), and (202) bands. The intensity of the different groups are not normalized with respect to one another. In the 525–495-nm region, the PHOFRY spectrum obtained by monitoring NO[$v''$=0, $Q_{22}$(33.5)] is much more intense than that obtained by monitoring the $P_{22}$ bandhead of NO($v''$=2).

**TABLE III: Spectroscopic Data for the $T_1 \leftarrow S_0$ and $S_1 \leftarrow S_0$ Transitions of ClNO**

| $v_1'$ | $v_3'$ | peak position,[a] nm | $\nu$, cm$^{-1}$ | $\Delta\nu$(fwhm), cm$^{-1}$ | $\tau$,[b] fs |
|---|---|---|---|---|---|
| | | | $T_1$[c] | | |
| 0 | 0 | 616 (615.8) | 16230 | 290 | 18.3 |
| 0 | 1 | 602 (601.7) | 16610 | 331 | 16.0 |
| 0 | 2 | 587 (587.9) | 17040 | | |
| 1 | 0 | 565 (561.2) | 17700 | 157 | 33.8 |
| 1 | 1 | 553 (549.5) | 18050 | 262 | 20.3 |
| 1 | 2 | 541 (538.5) | 18480 | 290 | 18.3 |
| 2 | 0 | 519 | 19270 | 74 | 71.8 |
| 2 | 1 | 509 | 19650 | 116 | 45.8 |
| 2 | 2 | 500 | 20000 | 201 | 26.4 |
| | | | $S_1$[d] | | |
| 0 | - | 472 (475.0) | 21186 | 1300 | 4.08 |
| 1 | - | 440 (440.0) | 22727 | 1000 | 5.31 |

[a] The numbers in parentheses are from ref 28. [b] $\tau$ is the lifetime associated with the fwhm line width. [c] From ref 23. [d] From ref 38.

and vector properties, show that in this region NO($v''$=1) is formed exclusively via $S_1 \leftarrow S_0$ excitation, whereas NO($v''$=0) is formed predominantly via $S_3 \leftarrow S_0$ absorption (Figure 5).

The absorption spectra can be converted to gradients of the potential along the $R$ coordinate.[40] Using measured line widths (Table III), we calculated the potential curves for $S_1$(000), $S_1$(100), $T_1$(001), and $T_1$(101) as shown in Figure 7. In constructing the curves we used the known energy values in the FC and asymptotic regions, and these regions are marked by heavy lines. In ClNO, as a consequence of the mismatch between the parent $\nu_1$ frequency (1500 cm$^{-1}$) and the free NO vibrational frequency (~1900 cm$^{-1}$), the curves in $S_1$ and $T_1$ become flatter with increasing $\nu_1$ quanta, giving rise to progressive narrowing of the absorption bands as a function of $v_1$. The lifetimes derived from the bandwidths reflect the propagation times of the initially prepared wavepacket in the excited electronic state out of the FC region and give only lower limits to the dissociation lifetimes. It is intriguing that a diffuse

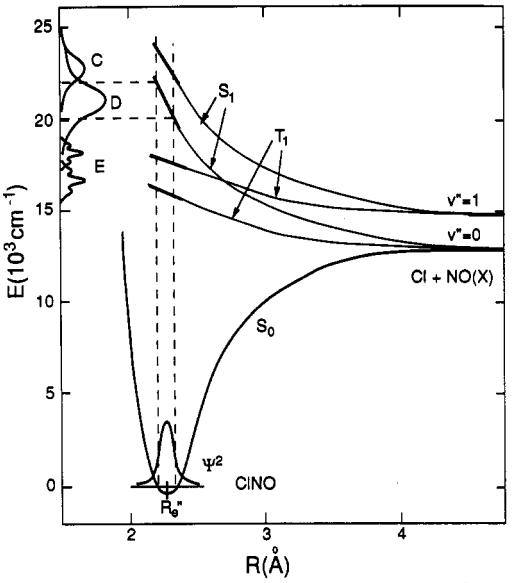


**Figure 7.** Pictorial representations of cuts in the ClNO potential surfaces in the $R$ coordinate near the Franck–Condon region. $R$ is the distance between the Cl atom and NO c.m. The two curves denoted by $S_1$ correspond to excitations in $S_1$(000) and $S_1$(100) that evolve asymptotically to NO $v'' = 0$ and 1, respectively, and the corresponding curves denoted by $T_1$ correspond to $T_1$(001) and $T_1$(101) excitations. The slopes in the Franck–Condon region are calculated by the "reflection principle" from the measured widths of the absorption bands, shown schematically on the left.

vibrational structure can exist even when the lifetime associated with the line width is shorter than a vibrational period (i.e., "direct" dissociation). This has been also shown theoretically for ClNO($S_1$) and $CH_3SNO(S_1)$.[37,41]

### 3. Photofragment Rotational Excitations

**The Franck–Condon Model for Photodissociation.** The basic idea behind the FC model for dissociation is the expansion of the parent molecular wave functions in terms of the final dissociative state wave function.[17–20] The squares of the expansion coefficients give the partial cross sections into each rotational state, and thus the diatomic rotational state distribution. Notice that the wave functions describing the dissociative state are not simply those of the free diatomic fragment, since in the dissociation the conserved quantities impose constraints on the relative motions of the two fragments.[19]

We start with the simple Franck–Condon treatment for triatomic photodissociation, ABC → A + BC, as developed by Beswick and Gelbart.[19] In their treatment, the stretching ($R$, $r$) and bending ($\theta$) motions of the parent are uncoupled, and the Hamiltonian describing the bending motion is

$$H = \frac{1}{2\mu_1 R^2} l^2 + \frac{1}{2\mu_2 r^2} j^2 + V(\theta) \qquad (1)$$

where j is the diatomic rotational angular momentum, l is the relative orbital angular momentum between the fragments, and $\mu_1$ and $\mu_2$ are the reduced masses of A–BC and BC, respectively. The Jacobi coordinates used in these calculations are shown in Figure 8A. In the theory, the bound wave functions are expanded in terms of simultaneous eigenfunctions of the operators $J^2$, **J·R**, **J·Z**, and $j^2$, where **J** = **l** + **j** is the total angular momentum, and $Z$ is a space-fixed axis, chosen to lie along the body-fixed axis $R$ (see Figure 8B). In particular, the bending states are represented by linear combinations of the diatom free-rotor wave functions, and stretching motions are uncoupled from fragment rotations. Although the theory is general and therefore applicable to all $J$'s, in photodissociation involving jet-cooled samples the total angular momentum is very small justifying the use of $J = 0$, thereby

(40) (a) Herzberg, G. *Spectra of Diatomic Molecules*; Van Nostrand: New York, 1950. (b) Herzberg, G. *Spectra of Polyatomic Molecules*; Van Nostrand: New York, 1966.

(41) Schinke, R.; Henning, S.; Untch, A.; Nonella, M.; Huber, J. R. *J. Chem. Phys.* **1989**, *91*, 2016.

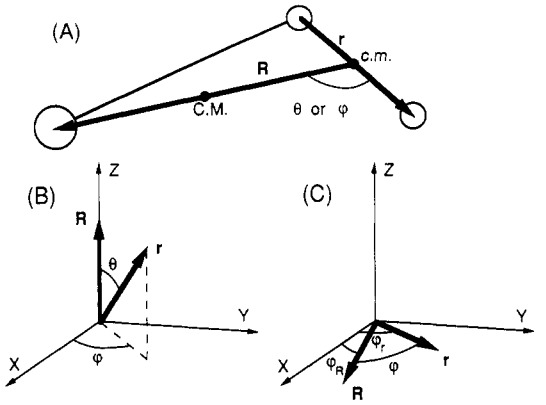


**Figure 8.** The coordinate systems used in the model calculations. The Jacobi coordinates are shown in (A). In (B) and (C), the molecule-fixed coordinate systems are shown; in (B) the $Z$ axis is aligned with $R$, whereas in (C) it is perpendicular to the molecular plane.

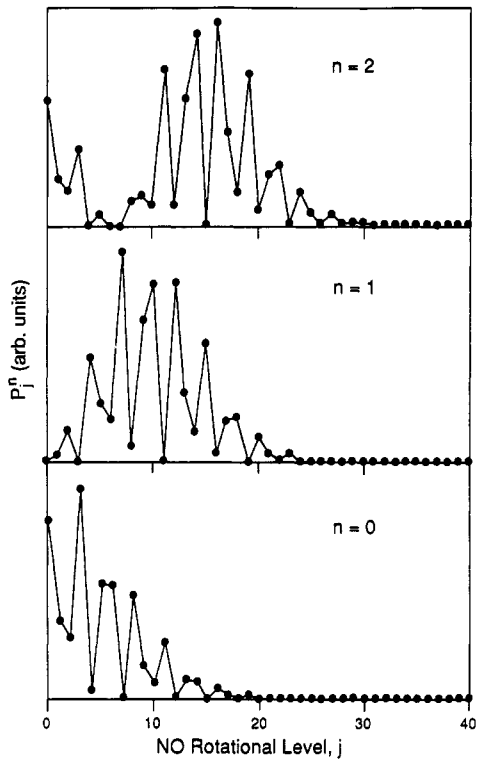


**Figure 9.** NO rotational distributions calculated from Franck–Condon projections of ClNO harmonic-oscillator bending wave functions in $T_1$ into free NO wave functions. The following bending parameters were used: $B$ = 1.96 cm$^{-1}$, $\omega$ = 380 cm$^{-1}$.

simplifying the equations considerably. The dissociative-state wave function in this case can be written as[19]

$$\Psi_{free} = Y_{j0}(\theta) \tag{2}$$

where the $Y_{j0}$ are spherical harmonics and $\theta$ is the body-fixed angle between **r** and **R**, as defined in Figure 8A. As noted above, $Y_{j0}$ is not the free-rotor wave function of the diatom, but the wave function describing the concerted motion of $R$ and $r$ when $J$ = 0.[19] The diatomic rotational distribution is given by the overlap integral between the bound and free wave functions

$$P_j^n = |\langle\Psi_{bound}|\Psi_{free}\rangle|^2 = |2\pi \int \sin\theta\, d\theta\, Y_{j0}(\theta)\, \phi_n(\theta)|^2 \tag{3}$$

where $\phi_n(\theta)$ is the bending wave function in quantum state $n$ in the ground or excited electronic state. In Figure 9, we display calculated rotational distributions for dissociation of ClNO assuming harmonic oscillator bending wave functions in the excited electronic state ($\omega_{bend}$ = 380 cm$^{-1}$ and $B$ = 1.96 cm$^{-1}$).

Morse and Freed obtained an expression similar to eq 3 by applying their analytical FC model to bent triatomics and using harmonic oscillator bending wave functions.[17] The rotational probabilities are given by[17]

$$P_j^n \propto \sin^2[j'\theta_0 + (-1)^n\pi/4] H_n^2(\alpha'^{1/2}j') \exp(-\alpha' j'^2) \tag{4}$$

where $j' = j + 1/2$, $\alpha'$ is a constant related to the bending frequency and bending moment of inertia, $H_n$ are the Hermite polynomials, and we set $\hbar$ = 1 throughout. The distributions obtained by using eqs 3 and 4 are similar, both exhibit a fast oscillatory term which depends strongly on the equilibrium bending angle $\theta_0$, and a slowly varying term given by the harmonic oscillator wave function squared with angular momentum argument. Equation 4, however, highlights the relation between the *rotational distribution* and the harmonic oscillator *bending wave function*, and also shows clearly the fast oscillatory factor (first term). We will come back to this last point later.

In our work, we took a slightly different approach to the FC expansion in cases where $J$ = 0, in order to highlight the physics. We chose a molecule-fixed coordinate system with the $Z$ axis perpendicular to the molecular plane defined by **R** and **r** as shown in Figure 8C. Using the addition theorem of spherical harmonics, we obtained the "free" wave function:[23]

$$\Psi_{free} = [4\pi/(2j+1)]^{1/2}\sum_m Y_{jm}^*(\theta_R=\pi/2,\varphi_R)\, Y_{jm}(\theta_r=\pi/2,\varphi_r)$$

$$= [4\pi/(2j+1)]^{1/2}\sum_m |Y_{jm}(\theta=\pi/2)|^2 \exp(im\varphi) = Y_{j0}(\varphi) \tag{5}$$

The corresponding rotational distribution for the diatomic fragment then becomes, for high $j$ levels[23,42]

$$P_j^n \approx 2\pi(|C_j^n|^2 + |C_{-j}^n|^2) + \text{interference terms} \tag{6}$$

where

$$C_m^n = (2\pi)^{-1/2} \int \exp(im\varphi)\, \phi_n(\varphi)\, d\varphi \tag{7}$$

Equation 6 has a simple physical interpretation; the rotations of the diatom arise from parent bending motions, where angle *opening* ($|C_j^n|^2$) and *closing* ($|C_{-j}^n|^2$) motions, which correspond to counterclockwise and clockwise rotations of the diatomic fragment, respectively, have equal probabilities. The interference terms between the two motions cause the fast oscillations which are strongly dependent on the bending angle, $\varphi_0$.

Notice also that since $C_m^n$ in eq 7 is the Fourier transform of the bending wave function in the coordinate representation, it represents the wave function in the angular momentum representation.[43] Recall that, owing to the symmetry of the harmonic oscillator Hamiltonian, its wave functions have the same functional form in both the coordinate and momentum representations.[43] This is precisely why in eq 4 the slowly varying factor is the square of the harmonic oscillator wave function with *angular momentum* argument. In Figure 10, we display the first three bending wave functions in both coordinate and momentum representations (i.e., $\phi_n(\varphi)$ and $C_m^n$) calculated for ClNO using the same parameters as in Figure 9.

As stated above, the interference terms in eqs 3, 4, and 6 cause fast oscillations in the rotational distributions (Figure 9). In photodissociation experiments, these oscillations will be rarely observed. They are strongly dependent on parent rotational levels, and since even under jet-cooled conditions a distribution of parent rotations is obtained, the oscillations will be averaged out.[44] In addition, it has been shown that in the actual dissociation the combined motions in the diatomic stretch ($r$) and the reaction ($R$) coordinates tend to wash out the fast oscillations.[44] Furthermore, the anisotropy in the bending potential (or torque), which changes $\varphi_0$ during dissociation, also smooths out the interferences.[45] This

(42) For high $j$'s, the summation in eq 5 reduces to two terms (i.e., $m = \pm j$), and since $|Y_{jj}(\theta = \pi/2)|^2[4\pi/(2j+1)]^{1/2}$ approaches a constant independent of $j$, we obtain eq 6. See ref 21 for details.

(43) (a) Merzbacher, E. *Quantum Mechanics*; Wiley: New York, 1961. (b) Landau, L. D.; Lifshitz, E. M. *Quantum Mechanics*; Pergamon: Oxford, 1977.

(44) (a) Grinberg, H.; Freed, K. F.; Williams, C. J. *J. Chem. Phys.* **1990**, *92*, 7283. (b) Grinberg, H.; Williams, C. J.; Freed, K. F., private communication.

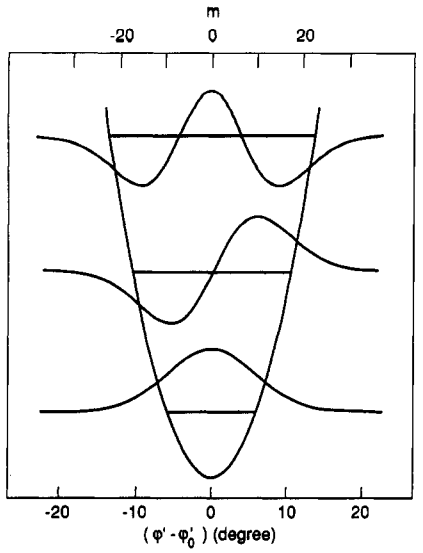


**Figure 10.** The harmonic-oscillator bending wave functions of ClNO($T_1$) used in the model calculations, presented both in coordinate ($\varphi$) and momentum ($m$) space. As expected, the shapes of the wave functions in the coordinate and momentum representations are identical, giving rise to nodes in the angular momentum probability functions which depend sensitively on the number of bending quanta.

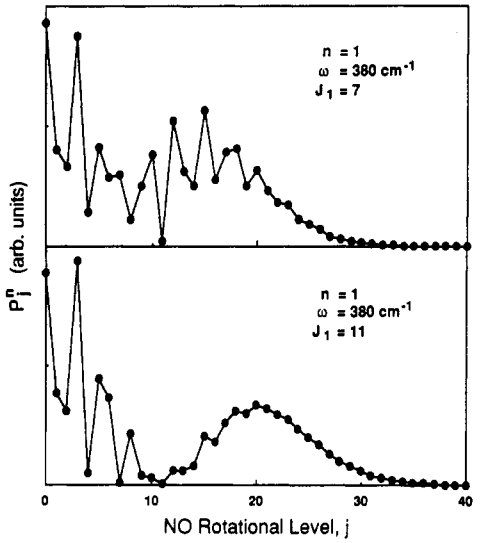


**Figure 11.** NO rotational distributions calculated from Franck–Condon projections of ClNO harmonic-oscillator bending wave functions in $T_1$ into free NO wave functions, but including external torques $J_1 = 7$ (upper panel) and 11 (lower panel).

is shown in Figure 11, where exit-channel torques, $J_1$, of 7 and 11 angular momentum units are introduced. The torque causes a shift in the rotational distribution to higher $J$ values (see below), but also smooths the fast oscillations. We are aware of only one case in which the fast oscillatory structure has been observed. In the dissociation of water on the first excited singlet state accessed from specific rotational levels of the (001) level of the ground electronic state, fast oscillations are observed which are well described by the FC model.[1c,46] In this case dissociation involves single parent rotational states, and exit-channel interactions are small. We emphasize that the FC model can be applied to cases where the mapped bending vibrational level is either in the excited or the ground electronic state. In the latter case, the only requirement is that the upper state be sufficiently repulsive to prevent the development of a bending wave function, and therefore it is the *ground*-state bending wave function which is expanded in terms of the rotor wave functions.[17-20]

By examination of the basic features of the harmonic oscillator Hamiltonian and its wave functions, further insight into the fragment rotational distributions can be obtained. For $J = 0$ (i.e., $\mathbf{l} = -\mathbf{j}$), the bending harmonic oscillator Hamiltonian can be written as

$$H = \frac{1}{2I}j^2 + \frac{I\omega^2}{2}(\varphi - \varphi_0)^2 \tag{8}$$

where $I$ is the bending moment of inertia defined by $I^{-1} = (\mu_1 R^2)^{-1} + (\mu_2 r^2)^{-1}$, and $\omega$ is the bending frequency. The corresponding wave functions in the angular coordinate representations are

$$\phi_n(\varphi) = \phi_n[(\omega I)^{1/2}(\varphi - \varphi_0)] \tag{9a}$$

where $\phi_n(x) = a_n H_n(x) \exp(-x^2/2)$ is the standard harmonic oscillator wave function. In the angular momentum representation, we obtain

$$C_m^n = \phi_n[m/(I\omega)^{1/2}] \tag{9b}$$

Comparisons of eqs 9b, 6, and 7 demonstrate that without the interference terms the rotational distribution is just half of the square of the bending wave function (corresponding to $m \geq 0$), and therefore depends sensitively on the number of bending quanta (e.g., compare Figures 9 and 10). Notice also that the widths of the bending wave functions in the two representations, $\Delta j$ and $\Delta\varphi$, are related by Fourier transformation. Since $\Delta j$ depends on $(I\omega)^{1/2}$, floppy molecules (i.e., those having small $I$ and/or small $\omega$) are spread out in space, and therefore associated with narrow angular momentum distributions, thus resulting in narrow rotational distributions.

**The Modified FC Model: Inclusion of Exit-Channel Torques.** The advantage of the FC model is its independence of the details of the dissociative PES. This simplicity also limits its applicability, since molecules dissociate on real PES's, and only in rare cases does the model predict correctly the rotational distributions. However, it is important to realize that the FC model always yields the *initial* angular momentum distribution inherent in the parent bending wave function. In the dissociation, this initial angular momentum distribution subsequently evolves under the influence of the PES into the observed product rotational distribution. As seen below, for fast dissociation the final rotational distribution may still reflect some of the characteristics of this initial distribution even in the presence of exit-channel torques.

For cases where only a modest torque is generated during the dissociation (e.g., the photodissociation of ClNO on $T_1$), we developed a simple physical picture which yields the fragment rotational distributions.[23,24] This is basically a modification of a simplified FC model, in which a small, uniform torque is treated in a time-dependent fashion. Here we give the general framework of the model and apply it to the photodissociation of ClNO($T_1$). The model treats the motion along the reaction coordinate $R$ classically and employs a time-dependent bending Hamiltonian. The time-dependent bending wave function at some critical time (i.e., critical $R$) is expanded as in the pure FC model. The angular anisotropy in the PES, and the couplings between different parent degrees of freedom are viewed as time-dependent parameters (i.e., the bending frequency, moments of inertia, and equilibrium angle all change during dissociation).

The time-dependent harmonic oscillator bending Hamiltonian is similar to eq 8

$$H(t,\varphi) = \frac{1}{2I(t)}j^2 + \frac{I(t)\omega^2(t)}{2}[\varphi - \varphi_0(t)]^2 \tag{10}$$

where $I^{-1}(t) = [\mu_1 R^2(t)]^{-1} + [\mu_2 \bar{r}^2(t)]^{-1}$, and $I(t)$ is defined as the time-dependent bending moment of inertia. $\bar{R}(t)$ and $\bar{r}(t)$ denote average values of $R$ and $r$ at any given time, and $\omega(t)$ and $\varphi_0(t)$ are the instantaneous bending frequency and equilibrium angle, respectively. As the molecule dissociates, one expects the bending force constant and therefore $\omega(t)$ to decrease rapidly. $\varphi_0(t)$ describes how the equilibrium bending angle changes during the dissociation, thus generating a unidirectional angular momentum

(45) (a) Schinke, R.; Engel, V.; Staemmler, V. *J. Chem. Phys.* **1985**, *83*, 4522. (b) Qian, C. X. W.; Reisler, H., unpublished work.

(46) Schinke, R.; Engel, V.; Andresen, P.; Häusler, D.; Balint-Kurti, G. G. *Phys. Rev. Lett.* **1985**, *55*, 1180.

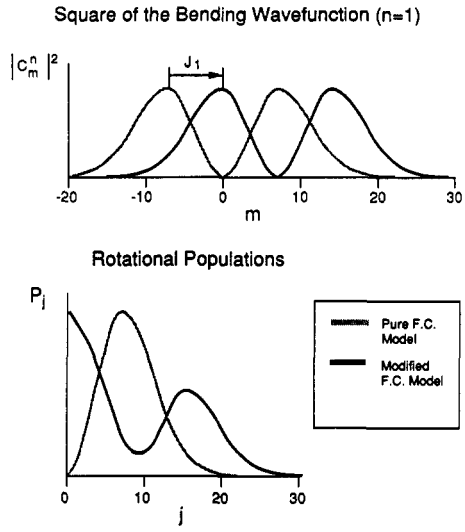


**Figure 12.** Pictorial representations of the correspondence between the parent bending angular-momentum wave functions (i.e., $C_m^n$) and the rotational populations, $P_j$. The light-shaded curves show the momentum eigenfunction centered at $m = 0$ (upper panel), and the corresponding rotational distribution obtained by using eq 6 and summing over $\pm j$ (lower panel). When a unidirectional torque $J_1$ is included, the modified FC model is used (solid lines). The upper panel shows the angular momentum wave function centered at $m = J_1$, which is obtained via Fourier transformation of eq 11. The rotational distribution shown in the lower panel is shifted relative to the one obtained without exit-channel torque.

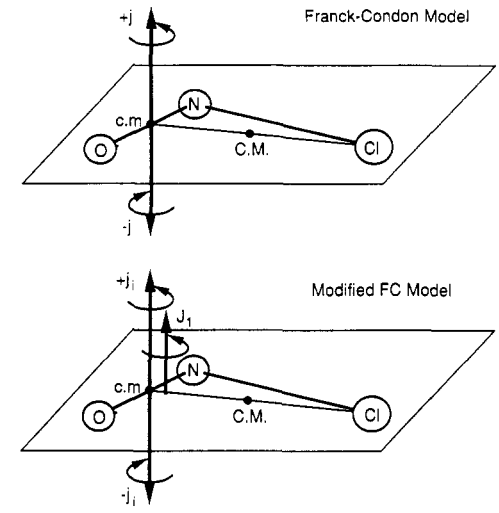


**Figure 13.** Pictorial representations of the sources of angular momentum giving rise to the observed NO rotational excitation. The bending wave function is the source of equal clockwise and counterclockwise rotation, $\pm j_1$. In contrast, the angular momentum $J_1$ generated by the anisotropy in the PES is unidirectional.

superimposed on the angular momenta that derive from the parent bending motion. Notice the similarities between eqs 10 and 8; if we set $\omega$ as a step function (i.e., $\omega$ is constant before dissociation, and equal to zero afterwards), and $I$ and $\varphi_0$ as constants, we obtain the pure Franck–Condon limit.[23] If $\omega$ decreases slowly with time, the wave functions will adiabatically follow the changing Hamiltonian. In this case, we use a weighted average of the bending frequency, $\bar{\omega}$ in eq 9. This rescales the width of the angular momentum distribution according to $(I\omega)^{1/2}$, and usually results in narrower angular momentum distributions, since $\bar{\omega}$ decreases with increasing $R$.

The time-dependent problem for equilibrium angle change (i.e., $\varphi_0$ as a function of time) can be solved analytically to yield the time-dependent wave functions[47]

$$\Psi_n(\varphi,t) = \exp\{iJ_1(t)[\varphi - \varphi_1(t)]\}\phi_n(\varphi - \varphi_1(t)) \qquad (11)$$

where

$$J_1(t) = (I\omega^2)\int_0^t \varphi_0(t') \cos \omega(t - t')\, dt' \qquad (12a)$$

$$\varphi_1 = \omega \int_0^t \varphi_0(t') \sin \omega(t - t')\, dt' \qquad (12b)$$

The corresponding momentum wave function squared is centered at $m = J_1$, i.e., *the angular momentum distribution is shifted in the direction of the torque generated by the change in the equilibrium bending angle during the dissociation.* The resulting rotational distribution, obtained by neglecting the interference terms [i.e., using only the first two terms in eq 6], is[23]

$$P_j^n = F[j - J_1(T)] + F[-j - J_1(T)] \qquad (13)$$

where $T$ is the time when the Franck–Condon expansion is carried out, and

$$F(x) = H_n^2[(I\omega)^{-1/2}x] \exp(-x^2/I\omega) \qquad (14)$$

In Figure 12, we show graphically how the rotational distributions are obtained from the wave functions given by eq 11, and in Figure 13 we show the superposition of torques.

(47) See, for example, *Problems in Quantum Mechanics*; ter Haar, D., Ed.; Pion Ltd.: London, 1975.

Thus, the initial angular momentum distribution inherent in the parent wave function is modified in two ways during the dissociation; its center is shifted from zero to $J_1$ due to the unidirectional torque, and its width is changed due to the change in the bending force constant. Most often, the wave function *spreads* in the angular coordinate during dissociation, thus giving rise to a *narrower* rotational angular momentum distribution than predicted by the pure FC model, as dictated by the uncertainty principle.

**Mapping of Bending Wave Functions: Application to the Photodissociation of ClNO($T_1$).** The photodissociation of ClNO on $T_1$ presents an opportunity for studying the influence of parent excited-state vibrational motion (both the stretch and the bend) on the dissociation dynamics. The experimental results show that the parent NO stretching vibration transforms adiabatically into fragment NO vibration, while the bending wave functions are mapped into fragment rotational distributions.[23] In addition, the NO rotational constants are small enough to provide a dense grid of angular momentum states and thus show clearly the correspondence between the bending wave functions and the rotational distributions.

The PHOFRY spectrum of ClNO in the region 525–625 nm consists of three groups of three peaks, assigned to progressions in the NO stretch, $\nu_1$, and bending, $\nu_3$, modes (Figure 6).[23] We find that excitations in the $T_1$ ($00v_3$), ($10v_3$), and ($20v_3$) levels lead predominantly to formation of NO in $v'' = 0$, 1, and 2, respectively. The rotational distributions of NO($^2\Pi_{3/2}$) were obtained at several photolysis wavelengths and are shown in Figure 14, uncorrected for alignment effects. Rotational distributions obtained for NO($v''=0$) and NO($v''=1$) are shown following excitation in the ($00v_3$) and ($10v_3$) bending progressions, respectively, and in each case the excitation wavelength coincides with a peak in the photofragment yield spectrum. The distributions depend sensitively on the number of bending quanta in the upper state but are independent of the number of NO stretch quanta.[15,23] Excitations in the ($20v_3$) bands result in similar distributions to those displayed in Figure 14.

The rotational distributions can be described by the modified FC model. Since the absorption spectrum exhibits diffuse vibrational structure, we assume that the excited-state vibrational wave functions are fully developed during the early stage of the dissociation. Therefore, to simplify the discussion, we divide heuristically the photodissociation of ClNO on $T_1$ into three steps:

$$\text{ClNO} + h\nu \rightarrow \text{ClNO}^* \qquad \text{(I)}$$

$$\text{ClNO}^* \rightarrow \text{ClNO}^{*\prime} \qquad \text{(II)}$$

$$\text{ClNO}^{*\prime} \rightarrow \text{Cl} + \text{NO} \qquad \text{(III)}$$

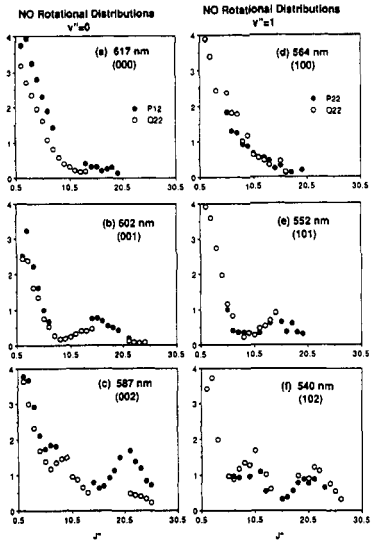


**Figure 14.** Nascent NO($X^2\Pi_{3/2}$) rotational level distributions obtained following excitation of jet-cooled ClNO at wavelengths corresponding to the peaks in the $T_1 \leftarrow S_0$ PHOFRY spectra (Figure 6). The upper, middle, and lower panels correspond to excitations of $v_3 = 0$, 1, and 2, respectively, in $T_1$. The panels on the left show the $P_{12}$ and $Q_{22}$ level distributions for NO($v''=0$), whereas those on the right show the $P_{22}$ and $Q_{22}$ distributions for NO($v''=1$). The results were obtained with $E_{pr} \parallel E_{ph}$, $k_{pr} \parallel k_{ph}$, and vertically polarized $E_{pr}$. The distributions are not corrected for alignment and Λ-doublet populations differences.

Step I is the usual laser excitation which gives rise to the observed absorption spectrum, as per the FC factors. As discussed elsewhere, the adsorption line widths reflect mostly the slopes in the excited-state PES in the dissociation coordinate (i.e., $R$), and therefore reveal how long the molecules spend near the FC region. Step II describes the evolution of the initially prepared excited state toward a "critical configuration" (i.e., the transition state), before the final fragment separation takes place. Step III is a fast departure of the fragments, and, in the absence of couplings between the dissociation coordinate and the other coordinates (i.e., bending and NO stretch), the transition-state wave functions in the non-dissociative coordinates are "frozen" at the beginning of this departure and can be expanded in terms of the dissociative-state wave functions as described above. The final product rotational excitations are a consequence of (i) the initial angular momentum distributions inherent in the parent bending wave functions (which depend strongly on the number of bending quanta and are established in step I), and (ii) the evolution of this initial distribution on the dissociative PES (i.e., steps II and III).

By use of the modified FC model with transition-state bending wave functions and neglecting the fast oscillations discussed above,[48] the observed rotational distributions can be simulated with two adjustable parameters, $J_1$ and $\bar{\omega}$ in eqs 13 and 14.[23,24] In Figure 15 we display the simulations and note that the best fits are obtained when: (i) $\bar{\omega}$ decreases from the value derived from the absorption and photofragment yield spectra (380 $cm^{-1}$) to ~190 $cm^{-1}$; and (ii) $J_1$ is bending-level dependent, i.e., the changes in $\varphi_0$ depend on the excited-state bending level. The best fits are obtained with $J_1 = 2 \pm 2$, $7 \pm 1$, and $10 \pm 1$ for $v_3 = 0$, 1 and 2, respectively, and the agreement with the experimental results is good.[48]

Without detailed knowledge of the $T_1$ PES and full quantum mechanical calculations, we cannot fully justify the parameters used in the simulations. However, the values of $\bar{\omega}$ and $J_1$ are sensible. The best fits require $\bar{\omega} = 190$ $cm^{-1}$, which is smaller than the bending frequency in the FC region (i.e., 380 $cm^{-1}$). As stated earlier, $\bar{\omega}$ controls the spread of the angular momentum distribution, but not its nodal structure; the latter is determined solely by the number of bending quanta.[23] The values of $J_1$ correspond

(48) Similar results are obtained when including the interference effects, but the nodal structure is then less apparent, and the agreement with the experimental results is less obvious.

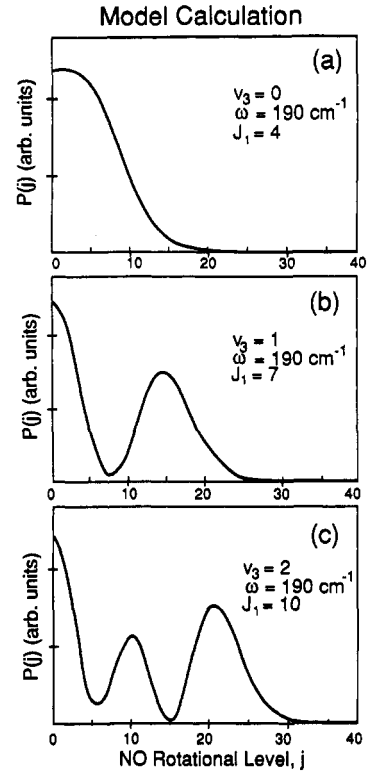


**Figure 15.** NO rotational distributions calculated for dissociation of ClNO on $T_1$ by using the modified FC model. The distributions were obtained by using a bending potential with effective frequency $\bar{\omega}$, and are shifted by torques, $J_1$, generated during the dissociation on $T_1$. The fast oscillations due to the interference terms were omitted (see the text for details).

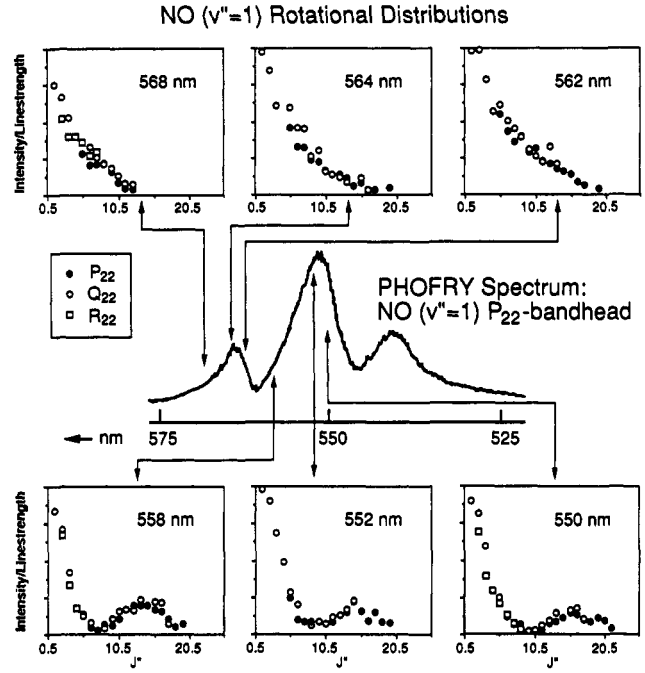


**Figure 16.** Rotational level distributions in NO($X^2\Pi_{3/2}$, $v''=1$) as a function of the dissociation wavelength in the (100) band (upper panels) and (101) band (lower panels) of ClNO($T_1$). The experimental conditions are the same as in Figure 14.

to changes of 2–7° in $\varphi_0$,[23] in good agreement with the ab initio calculations.[15] Comparison of Figures 14 and 15 shows that the experimental rotational distribution is distorted compared with the calculated one in that the first low $J''$ peak is higher relative to the second peak compared with the calculated distribution. This distortion probably occurs during step II, the evolution of the bending function on the PES toward the transition state.

The sensitivities of the rotational distributions to the unidirectional torque are shown also in Figure 16, where we display NO rotational distributions obtained when tuning the photolysis laser to different regions within the (100) ← (000) and the (101) ← (000) bands of the $T_1 \leftarrow S_0$ transition. The distributions corresponding to the red wings of the absorption bands are shifted to lower $J$'s. The model we developed assumes that most of the external torque develops along the reaction coordinate away from the FC region, and therefore the FC expansion is done at a "critical configuration" where the bending force constant is already small. Using the "reflection principle" for the dissociative absorption spectrum in the $T_1 \leftarrow S_0$ system (Figure 7), we realize that the red-wing excitations correspond to dissociation initiated at larger internuclear separations, $R$, than the blue-wing excitations. The average change in the rotational excitation only amounts to $\Delta J_1 \sim 2$ for dissociation in the (101) band, as compared with a total $J_1 = 7$ needed to simulate the experimental results. Thus the data suggest that the coupling between translation and bending, which is the source of $J_1$, is weak in the FC region, and most of the external torque is developed at larger Cl–N separations. Notice also that the ratio of the two peaks in the rotational distributions displayed in the lower panels of Figure 16 changes with excitation wavelength, demonstrating the dependence of the evolution of the bending wave function on the initial conditions. More accurate knowledge of the PES is clearly needed for more detailed simulations of the experimental results.

The NO rotational distributions from the dissociation of ClNO($T_1$) were the first to show the mapping of the excited-state bending wave functions.[23] Our ability to observe such a clear correspondence between the bending wave functions and the rotational distributions derives from some unique features of the $T_1$ PES. It is rather flat in the N–Cl coordinate near the Franck–Condon region, and vibrations are supported in the bending and NO stretch coordinates. It is, however, repulsive in the $r_{N-Cl}$ coordinate, resulting in fast, "direct" dissociation. The evolutions of the vibrational coordinates are to a large extent uncoupled, and the final-state interactions do not distort significantly the mapping of the bending wave function. Also, the absence of contributions from parent rotations in the jet-cooled samples adds to our ability to identify unambiguously the origins of the NO rotational excitations. The rotational distributions obtained with room temperature samples exhibit a much less pronounced structure, with the 'nodes' almost filled.[49]

**Bending Wave Functions and Large Exit-Channel Torques.** When final-state interactions are dominant, the rotational distributions are often well described by the semiclassical rotational reflection principle (RRP) developed by Schinke.[22] The rotational excitation is obtained by reflecting the initial bending wave function in the *coordinate* representation into the final angular momentum states of the fragment via the classical excitation function $J(\varphi)$. There are a number of excellent recent reviews describing RRP,[22,26] and therefore only a brief description will be given here.

The rotational excitation function $J(\varphi)$ is calculated by using classical trajectories on the excited state PES (usually assuming that the initial angular momentum is equal to zero). This excitation function $J(\varphi)$ reflects the torque that the diatomic molecule accumulates during dissociation, and establishes a classical mapping between the parent bending angle $\varphi$ and the fragment angular momentum $j$. The bending wave function squared (in the coordinate representation) then gives the corresponding weighting factor for each $j$. Finally, the rotational state distribution of the diatomic fragment is given by

$$P(j) = \sin [\varphi(j)]\ \phi_{bend}^2[\varphi(j)]\left|\frac{dJ}{d\varphi(j)}\right|^{-1} \qquad (15)$$

where $\varphi(j)$ is given by the inverse of the rotational excitation function.

$$j = J(\varphi); \quad \varphi(j) = J^{-1}(j) \qquad (16)$$

(49) Ogai, A.; Qian, C. X. W.; Reisler, H., unpublished work.

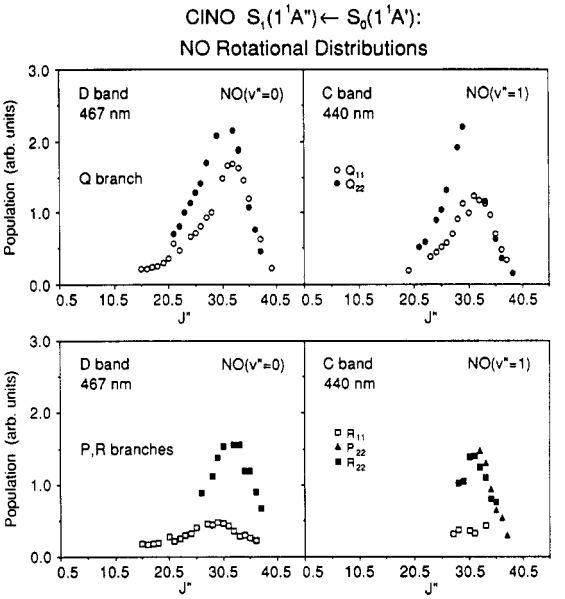


**Figure 17.** NO $v'' = 0$ and 1 rotational populations obtained upon excitation of ClNO to $S_1(1^1A'')$. The 11 and 22 subscripts refer to lines originating in the $^2\Pi_{1/2}$ and $^2\Pi_{3/2}$ states of NO, respectively. D band excitation to $S_1(000)$ yields predominantly NO in $v'' = 0$ while C band excitation to $S_1(100)$ yields predominantly NO in $v'' = 1$. For each vibrational level, the relative scales of the upper and lower panels are identical, while the relative populations of $v'' = 0$ and 1 are not normalized. The available energies with 467- and 440-nm excitations are 8413 and 7867 $cm^{-1}$, respectively.

Notice that RRP, being a semiclassical theory, uses a *classical* direct mapping between the parent bending *angle* and the final fragment angular momentum. It works best when the initial angular momentum inherent in the bending wave function is small relative to the external torque and the width of the fragment rotational distribution is determined predominantly by the excitation function. It has been very successful in a large number of cases including the dissociation of ClNO on $S_1$.[37a] For this fast dissociation, the bending wave functions in the excited states do not have time to develop. The rotational distributions across the D and C bands peak at $J'' = 31.5$ (see Figure 17) and are typical of those arising from dissociation on a surface with a large angular anisotropy. Schinke et al. performed both classical and quantum mechanical calculations on $S_1$ and reproduced well the experimental results.[37]

A simple impulsive model calculation, however, does not agree with the experimental results, since it yields a distribution peaking at $J'' = 40.5$ which is also much broader than the experimental distribution.[38] Schinke et al. find that the final rotational distribution is governed by two factors: (i) the impulsive force along the Cl–N bond that causes closing of the angle during the bond scission, and (ii) the anisotropy in the exit-channel angular potential which has a counteracting effect in inhibiting free rotation.[37] A detailed look at the $S_1$ PES shows that it is rather isotropic in the vicinity of the equilibrium angle where the dissociation commences. Consequently, rotation of NO is induced initially by the impulsive force acting between Cl and N. However, as NO starts to rotate, the anisotropy in the PES hinders free rotation of NO around its c.m. Since the two forces act in opposite directions, the final rotational excitation of NO is smaller than predicted by the impulsive model.[37] Thus, the net direction of the force does not coincide with the Cl–N bond, but is directed farther toward the c.m. of NO.

Both the RRP and the quantum mechanical calculations show that the width of the parent vibrational probability density on the ground electronic state is not directly reflected in the width of the rotational distribution; rather, the original wavepacket prepared in the Franck–Condon region subsequently propagates under the influence of the forces on the $S_1$ PES. The motion of the wavepacket can be divided into two parts; the center of the wavepacket follows a classical trajectory, thereby developing angular

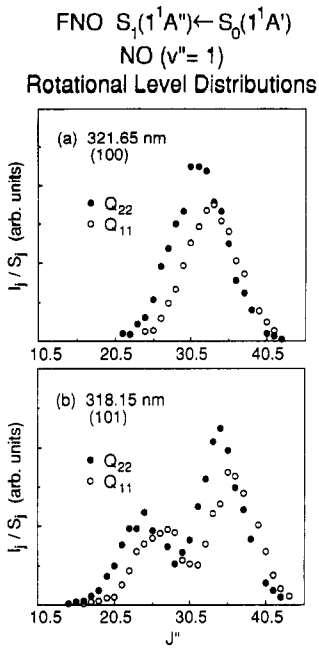


**Figure 18.** Nascent NO($X^2\Pi_{1/2}$) and NO($X^2\Pi_{3/2}$) rotational level distributions ($Q_{11}$ and $Q_{22}$ lines, respectively) obtained following excitation of jet-cooled FNO at wavelengths corresponding to (100) and (101) levels in $S_1$ (panels a and b, respectively). In both cases the $Q_{22}$ and $Q_{11}$ line intensities are divided by the corresponding line strengths.

momentum, while the size of the wavepacket may also change in the angular coordinate during the dissociation. Most often, as per the uncertainty principle, an increase in size of the wavepacket is accompanied by a decrease in the momentum spread, giving rise to a narrower final rotational distribution. The broadening of the wavepacket can also be seen in the calculations which show that the dissociation wave function spreads out as $R$ increases but is still centered along the reaction coordinate.[37] Thus, the dissociation of ClNO on $S_1$ provides an example in which the initial impulse, described by the reference impulsive model, is modified by the detailed evolution on the PES along the reaction coordinate. Both classical (RRP) and quantum mechanical calculations provide a detailed description of the rotational distribution.[37]

Particularly intriguing is a case where the bending wave functions in the excited state are well developed, and in addition a large impulsive force yields high rotational excitation. Such a situation exists in the dissociation of FNO($S_1$). FNO shows an extensive progression in the NO stretch [($v_1$00); $\nu_1 \simeq 1000$ cm$^{-1}$], but in addition, a second feature corresponding to ($v_1$01) ($\nu_3 \simeq 350$ cm$^{-1}$) appears to the blue of each ($v_1$00) peak.[50-52]

Our preliminary results on the photodissociation of FNO($S_1$) are displayed in Figure 18. The NO($^2\Pi$) $v'' = 1$ rotational distribution obtained upon excitation of FNO[$S_1$(100)] is quite similar to that obtained in the dissociation of ClNO[$S_1$(100)].[52] However, upon excitation of FNO[$S_1$(101)], a distinct bimodal rotational distribution appears (Figure 18b),[52] which looks qualitatively like a modified $v_3' = 1$ bending wave function shifted by $J_1 \simeq 30.5$ (see Figure 12). The shift should be well described by a semiclassical theory such as RRP, but the *shape* maps the shape of the *transition-state* wave function in the excited state, and the asymmetry in the rotational distribution reflects the propagation of the wave function toward the transition state. Preliminary ab initio calculations show a very shallow well in the $R$ coordinate.[53] Since FNO is isoelectronic with HONO, it is instructive to mention in this context that Schinke et al. carried out calculations using an approximate PES for HONO($S_1$), and showed that bending levels on $S_1$, which live for about 10 vibrational periods, evolve into NO rotational distributions peaking at high $J''$ under the influence of the large anisotropy in the repulsive part of the PES.[54] Despite the existence of large final-state interactions, the distributions preserve the memory of the nodal structure of the excited-state bending wave functions. The shape of the NO rotational distribution calculated for the dissociation of HONO($S_1$) with one quantum of bending excitation is quite similar to the NO distribution observed for FNO[$S_1$(101)]. Very recent calculations on the FNO($S_1$) PES yield excellent agreement with the results of Figure 18.[55]

## 4. Concluding Remarks

The classification presented here of sources of angular momenta and their contributions to the fragment rotational distributions is general, and our recent work shows that in many cases fragment rotational excitations can be understood with physically intuitive models. The initial impulse, bending wave functions, and exit-channel interactions all conspire to yield the final fragment rotational distributions, as shown in recent detailed calculations. The mapping of the parent bending wave functions into rotational distributions illustrated here is not limited to excited-state wave functions and small final-state interactions. As discussed by Freed and co-workers, the mapped wave functions can also be in the *ground* electronic state, especially in situations when there is no structure in the repulsive excited state (i.e., fast, direct dissociation).[17,18] Recently, oscillations in OH($X^2\Pi$) rotational distributions obtained in the dissociation of $H_2O$ initially excited to combination bands in the ground electronic state were observed and interpreted as reflections of the shapes of the bending wave functions in the *ground* state.[56] Also, as discussed above, in favorable cases even when a large impulsive force does exist, the shapes of the excited-state bending wave functions can still be reflected in the product rotational distributions.[52,54] However, the mapped wave functions are not necessarily those in the Franck–Condon region, but may be the wave functions of the transition state. More important, the distortions in the shapes of the wave functions are manifestations of final-state interactions and can be interpreted in terms of the PES along the reaction coordinate. We also note that often direct dissociation leads to inverted, "bell-shaped" rotational distributions that "reflect" the ground-state bending wave function but are still sensitive to the shape of the PES. We believe that many of these systems (e.g., ClCN,[57] $H_2O_2$[58]) will also exhibit mapping of bending wave functions when excited to higher bending levels in their ground electronic states, and the exact shape of the rotational distributions will reflect the dissociation dynamics and the propagation of the wavepacket to the transition state. The situation is more involved for predissociative systems; here both the couplings of the vibrational and translational degrees of freedom in the exit-channel and the dissociation time will determine whether the shape of the bending wave function will still be preserved to some extent in the final rotational distribution. We are currently studying the direct and vibrational predissociation channels of FNO($S_1$) and will compare the NO rotational distributions arising from the direct vs the predissociation channels. The experimental data, combined with knowledge of the PES and calculations of the dissociation dynamics, yield accurate information on the relationship between the electronic and nuclear motions. The physically intuitive models described in this article, present a qualitative way to interpret the data, and can also be predictive.

(50) Johnston, H. S.; Bertin, Jr., H. J. *J. Mol. Spectrosc.* **1959**, *3*, 683.
(51) (a) Solgadi, D.; Flament, J. P. In *Photophysics and Photochemistry Above 6 eV*; Lahmani, F., Ed.; Elsevier: Amsterdam, 1985; p 497.
(52) Ogai, A.; Brandon, J.; Reisler, H., to be published.
(53) Bai, Y. Y.; Reisler, H., unpublished work.
(54) Schinke, R.; Untch, A.; Suter, H. U.; Huber, J. R. *J. Chem. Phys.*, in press.
(55) Schinke, R., private communication.
(56) Schinke, R.; Vander Wal, R. L.; Scott, J. L.; Crim, F. F. *J. Chem. Phys.* **1991**, *94*, 283.
(57) (a) Barts, S. A.; Halpern, J. B. *J. Phys. Chem.* **1989**, *93*, 7346. (b) Schinke, R. *J. Chem. Phys.* **1990**, *92*, 2397. (c) Schinke, R.; Engel, V. *Faraday Discuss. Chem. Soc.* **1986**, *82*, 111.
(58) Grunewald, A. U.; Gericke, K. H.; Comes, F. J. *J. Chem. Phys.* **1988**, *89*, 345.

In conclusion, the current state-of-the-art theoretical and experimental developments in photodissociation dynamics have led to a much better understanding of the relationship between the electronic motions (PES) and nuclear motions (product state distributions). The advances made in recent years allow us to describe certain types of direct photodissociation processes within a more general, predictive framework, and this understanding should in turn form the basis for better control of photoinitiated reactions and other photoselective processes.

*Acknowledgment.* We have benefited greatly from discussions and correspondence with R. Schinke, R. B. Gerber, M. D. Morse, K. F. Freed, M. Shapiro, C. Wittig, Y. Chen, and G. A. Segal. We thank Lori Iwata-Hodgson for her excellent contributions to the early work. We are also grateful to R. Schinke for communicating results prior to publication and for ongoing in-depth discussions. The research is supported by the National Science Foundation and the Army Research Office under the auspices of the Center for the Study of Fast Transient Processes.

# ARTICLES

## "Memory Effects" in Molecular Fragmentation Induced by Site-Specific Core Excitation Using a Reflectron Time-of-Flight Mass Spectrometer

**Wieland Habenicht, Hermann Baiter, Klaus Müller-Dethlefs,* and Edward W. Schlag**

*Institut für Physikalische und Theoretische Chemie, Technische Universität München, Lichtenbergstrasse 4, D-8046 Garching, F.R.G.* *(Received: June 18, 1990)*

Bond-selective fragmentation of the molecules $CF_2{=}CH_2$ and $CF_3{-}CH_3$ is observed for site-specific C(1s) excitation. Excitation at either the fluorinated or hydrogenated C atom of $CF_2{=}CH_2$ and $CF_3{-}CH_3$ shows that the molecule memorizes the initial site of energy deposition, hence a chemical "memory effect". To follow the site-specific fragmentation channels, we employ a new "zero kinetic energy (ZEKE)" photoelectron–photoion coincidence technique using monochromatized X-ray synchrotron radiation from BESSY. The detection of ZEKE electrons serves to select the specific excitation of a carbon atom within the molecule. The fragmentation channels were assigned with high mass resolution by using a reflectron time-of-flight mass spectrometer.

### 1. Introduction

The search for bond-selective chemistry has received considerable attention during the past two decades. The excitation of inner-shell orbitals in molecules by soft X-ray synchrotron radiation offers a particular advantage since core orbitals like C(1s), N(1s), etc. are generally strongly localized at a specific atom and virtually do not participate in the chemical bonding. For the same kind of atom a *site-specific* excitation (i.e., the formation of a $1s^{-1}$ core hole localized at a specific atom) is made possible due to the "chemical shift".[1] This shift in energy of the 1s inner-shell orbitals for different ligands can be interpreted as an electron correlation effect between the valence electronic structure and the core level which depends on ligand properties like their electronegativity. For example, the binding energy of the $C_F(1s)$ orbital of fluorinated hydrocarbons is some electronvolts higher compared to the $C_H(1s)$ orbital (see section 3). To understand bond-selective chemistry and core electron excitation, it is of great interest to determine whether fragmentation channels depend on the *site of excitation* or whether randomization of energy distribution destroys the molecule's *memory* of the excitation process.

Site-specific fragmentation processes in acetone following C 1s → Rydberg orbital and 1s → $\pi^*$ excitation were first reported by Eberhardt et al.[2,3] in a mass spectrometric study using monochromatized tunable synchrotron radiation. In this example, the 1s → $\pi^*$ transition leads to a localized $C_O(1s^{-1})$ core hole (i.e., site selectivity), since the total cross section in the below-threshold region is dominated by that resonance. The fragmentation patterns observed in the $\pi^*$ resonance were quite different from those observed in the threshold region. Other studies on site-selective fragmentation processes were carried out by Nenner et al.,[4] Murakami et al.,[5] and Murphy et al.[6] Many aspects of chemistry induced by core orbital excitation were recently reviewed by Hanson.[7] The trend of such investigations is to use electron–ion coincidence techniques[8-11] and to resolve specific channels, e.g., by use of Auger electron–photoion coincidences[5-7,12,13] or by photoion–photoion coincidences.[14,15]

* To whom correspondence should be addressed.

(1) Siegbahn, K.; Nordling, C.; Johansson, G.; Hedman, J.; Hedén, P. F.; Hamrin, K.; Gelius, U.; Bergmark, T.; Werme, L. O.; Manne, R.; Baer, Y. *ESCA Applied to Free Molecules*; North-Holland: Amsterdam, 1969.
(2) Eberhardt, W.; Sham, T. K.; Carr, R.; Krummacher, S.; Strongin, M.; Wend, S. L.; Wesner, D. *Phys. Rev. Lett.* **1983**, *50*, 1038.
(3) Eberhardt, W.; Sham, T. K. *Proc. SPIE* **1983**, *447*.
(4) Nenner, I.; Morin, P.; Lablanquie, P.; Simon, M. *J. Electron Spectrosc. Relat. Phenom.* **1990**, *52*, 623.
(5) Murakami, J.; Nelson, M. C.; Anderson, S. L.; Hanson, D. M. *J. Chem. Phys.* **1986**, *85*, 5755.
(6) Murphy, R.; Eberhardt, W. *J. Chem. Phys.* **1988**, *89*, 4054.
(7) Hanson, D. M. *Adv. Chem. Phys.* **1990**, *77*.
(8) Brehm, B.; Puttkamer, E. v. *Z. Naturforsch.* **1967**, *22A*, 8; *Adv. Mass Spectrom.* **1968**, *4*, 591.
(9) Puttkamer, E. v. *Z. Naturforsch.* **1970**, *25A*, 1062.
(10) Eland, J. H. D. *Int. J. Mass Spectrom. Ion Phys.* **1972**, *8*, 143.
(11) Danby, C. J.; *Eland*, J. H. D. *Int. J. Mass Spectrom. Ion Phys.* **1972**, *8*, 153.
(12) Hayes, R. G.; Eberhardt, W. *J. Chem. Phys.* **1991**, *94*, 397.
(13) Hanson, D. M.; Ma, C. I.; Lee, K.; Lapiano-Smith, D.; Kim, D. Y. *J. Chem. Phys.* **1990**, *93*, 9200.
(14) Codling, K.; Frasinski, L. J.; Hatherly, P. A.; Stankiewicz, M. *Phys. Scr.* **1990**, *41*, 433.

0022-3654/91/2095-6774$02.50/0 